Available online at www.sciencedirect.com
SCIENCE DIRECT
International Journal of Heat and Fluid Flow 27 (2006) 636–643
International Journal of HEAT AND FLUID FLOW
www.elsevier.com/locate/ijhff

Mixing analysis of a swirling recirculating flow using DNS and experimental data

Martin Freitag *, Markus Klein, Mark Gregor, Dirk Geyer, Christoph Schneider, Andreas Dreizler, Johannes Janicka

Fachgebiet Energie und Kraftwerkstechnik, Technische Universitt Darmstadt, Petersenstr. 30, Darmstadt, D-64287, Germany

Available online 30 March 2006

Abstract

Fluid flow and mixing of a recirculating, swirling flow at moderate Reynolds number was investigated by direct numerical simulation (DNS) as well as experimentally using laser Doppler velocimetry (LDV) and spontaneous Raman scattering. Using these techniques together allows for a cross validation of the data. Furthermore, each technique can compensate for the restrictions of the other making the full data set more complete. Detailed one and two point statistics for velocity and scalar concentration are presented and discussed. The high swirl momentum leads to a fluid mechanical instability, a so-called precessing vortex core (PVC), which will be characterized especially with respect to its interaction with the scalar field. The results show that due to the reverse flow zone the PVC strongly modifies the mixing process leading to a precessing scalar concentration field. However, the level of the mean square deviation for the scalar field is considerably smaller than the corresponding value for the velocity field due to the different nature of the radial mean velocity and scalar concentration profiles in the near nozzle region.

Keywords: Direct numerical simulation; Spontaneous Raman scattering; Scalar mixing; Strongly swirled flow; Precessing vortex core

1. Introduction

Fluid-mixing by turbulent motion is of great importance for processes such as heat and mass transfer or chemical reaction. The effect of swirl can enhance mixing drastically and also it can be used to stabilize premixed flames in an inherent way. Therefore, the prediction methods used for this type of flows—RANS, URANS and LES— must be assessed in their quality. For this purpose, direct numerical simulation (DNS) is ideally suited at moderate Reynolds numbers to create a database for quality assurance and also to provide comprehensive information to scientists and engineers.

The investigation of swirl flows, experimentally as numerically, in a wide range of Reynolds numbers, has been an ongoing effort during the last fifty years. A detailed description on the phenomena of vortex breakdown caused by swirling motion can be found in Syred and Beer (1972) or Fahler and Leibovich (1977). Recently, a large number of publications within this subject has been summarized in the review of Lucca-Negro and O'Doherty (2000). Often swirl flows exhibit large coherent structures of vortex type, which perform a precessing motion (precessing vortex core, PVC), if the swirl number is sufficiently high. This phenomenon, initially documented by Chanaud (1965), has been observed to occur in isothermal flows, premixed and non premixed combustion. If the investigated swirl flow is running under premixed combustion conditions, the coherent structure can cause a feedback mechanism with acoustic modes, resulting into back-stroke of the flame into the nozzle.

In the work of Ruith et al. (2003), DNS was used to investigate the phenomena of vortex breakdown at a swirling flow of very low Reynolds number ($Re = 200$). Also the authors compared different visualization techniques, considering the question, if they really identify the PVC or only the turbulent shear stresses. Freitag and Klein (2005) studied a turbulent swirling flow by means of a DNS and

* Corresponding author. Tel.: +49 6151 165334; fax: +49 6151 166555.
E-mail address: mfreitag@ekt.tu-darmstadt.de (M. Freitag).

0142-727X/$ - see front matter © 2006 Elsevier Inc. All rights reserved.
doi:10.1016/j.ijheatfluidflow.2006.02.020

characterized the flow field in terms of one and two point statistics. The precessing vortex core was quantified using frequency analysis and spatial two point correlations.

The considerable progress in the application of the large eddy simulation (LES) approach to increasingly complex geometries can be found also in various publications on swirl flows. Exemplary we like to mention the excellent results with swirled co-axial jets (Pierce and Moin, 1998), who also predict a scalar concentration. Promising results of an isothermal swirl flow with recirculation have been published by Tang et al. (2002), García-Villalba and Fröhlich (2005) and Lu et al. (2005), who also considered the generation of acoustic waves caused by the impact of the vortical motion. Wegner et al. (2004) documented LES and URANS of the identical swirler device.

In order to develop better modeling strategies for such complex flows, going beyond the gradient flux approximation with its well known deficiencies, corresponding DNS data would be highly desirable. But direct simulations including scalar transport were mostly performed for relatively simple configurations, so far (see e.g., Hattori et al., 2003; Kim and Moin, 1989; Klein et al., 2004).

This paper presents a first attempt in setting up a DNS database of more complex configurations, and will be used in the future for testing (1) a newly developed model for the turbulent scalar flux (see Klein et al., 2004), as well as (2) strategies for assessing the quality of large eddy simulations (Klein, 2005).

2. Setup and measurement technique

The experimental setup consists of a movable block type swirler, which feeds an annulus from where the airflow enters the measurement section at ambient pressure and temperature. A principal sketch of the swirler device is presented in Fig. 1. More details can be taken from Schneider et al. (2005) and Freitag and Klein (2005).

Transient velocities have been measured by two-dimensional LDV in back scatter mode. A mixture of MgO and $ZrSiO_4$ served as seeding material. Along axial and various radial profiles statistical moments have been deduced from about 10 000 independent events per measurement point. Additionally, autocorrelations were deduced from time-series using the fuzzy slotting technique, local normalization, and transit time weighting (Maanen et al., 1999). Respective time scales and power spectra have been estimated by integration and Fourier transformation, respectively.

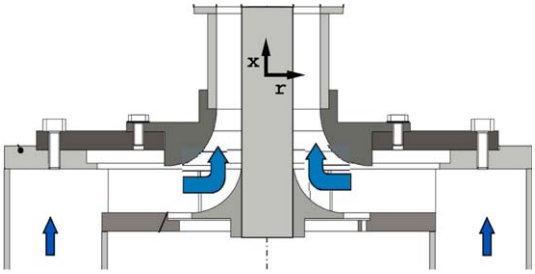

Fig. 1. Sketch of the swirler device.

Mixing fields were determined by one-dimensional Raman scattering. As passive scalar methane (5 vol.% in air) was used. For Raman scattering a cluster of four quality-switched frequency-doubled Nd:YAG lasers in addition with an optical delay line served to deliver a pulse train approximately 350 ns long containing an energy of 1.2 J. The measurement volume extended 5.6 mm in direction of the laser beam pointing. Ro-vibrational Raman bands of CH_4, N_2 and O_2 were imaged perpendicularly onto a slit of a Czerny-Turner type spectrometer by means of a custom-designed achromatic corrected $f\# = 2$ lens system (Geyer et al., 2004). Raman spectra were recorded by a thermo-electrically cooled backside illuminated CCD camera with low noise. The camera read-out time limited the repetition rate to approximately 1 Hz. To allow for single-shot measurements the CCD detector was gated by an ultra-fast mechanical shutter assembly (10 μs long gates). Binning in spatial direction resulted in 16 adjacent measurement "points" along the ID measurement volume with a spatial resolution of $400 \times 400 \times 400\ \mu m^3$ each. Data evaluation of single-shot measurements was based on spectral fitting of theoretical Raman spectra (Geyer and Dreizler, 2004) to experimental spectra delivering transient local mixing of the passive scalar. Using 600 single-shots at each measurement location, the first two statistical moments were extracted from the data. The precision of mean mixture fraction was 0.7%. Radial profiles were recorded at axial heights of 10, 20, 30, 60, and 90 mm.

3. Numerical technique and configuration

The governing equations for the investigated problem are the conservation equations of mass and momentum (1) for an incompressible Newtonian Fluid in their instantaneous local form, as well as the transport equation for a passive scalar (2).

$$\frac{\partial u_i}{\partial x_i} = 0$$

$$\frac{\partial u_i}{\partial t} + \frac{\partial}{\partial x_j}(u_i u_j) = \frac{\partial}{\partial x_j} v\left(\frac{\partial u_i}{\partial x_j}\frac{\partial u_j}{\partial x_i}\right) - \frac{1}{\rho}\frac{\partial p}{\partial x_i} \tag{1}$$

$$\frac{\partial c}{\partial t} + \frac{\partial}{\partial x_j}(c u_j) = \frac{v}{Sc}\frac{\partial^2 c}{\partial x_j^2} \tag{2}$$

The molecular diffusion coefficient of the scalar transport equation, is expressed by the ratio of kinematic viscosity and the Schmidt number (Sc), which was set to 0.7 in the calculation. The variables are located on a staggered, cylindrical grid, where the passive scalar c and the pressure are stored at the cell center. All equations are solved by using a finite volume technique. For spatial discretization second order central differences are used for the momentum equation. The convective fluxes of the scalar equation are discretized using a nonlinear TVD-limiter-scheme (CHARM) (PHOENICS, 2002), to keep the solution

bounded, and to avoid unphysical oscillations in the concentration field. The temporal discretization is an explicit third order Runge–Kutta-method and the Poisson equation is inverted by using a direct fast elliptic solver.

To allow recirculating fluid entering the nozzle, at least part of the nozzle has to be included in the computational domain. Due to the fact that the solver is of single block structure, immersed boundaries (Saiki and Biringen, 1996) are used to mimic the nozzle. Hereby, the walls of the nozzle are expressed by an artificial force added to the momentum equation. This force has been added to the velocities after the pressure correction at every Runge–Kutta time step.

The computational domain extends 12D in axial (x) and $8D$ in radial (r) direction and is resolved with $720 \times 256 \times 240$ ($\approx 44.23 \times 10^6$) grid nodes. Axially 2D are allocated to the annular part of the swirler. Except for the inflow boundary the domain is open at all other boundaries. Neumann boundary conditions for the velocity and the pressure are prescribed at the outflow, negative velocities are clipped. At the encompassing boundaries, velocities are treated with Neumann conditions and the pressure is set to be equal zero which allows mass entrainment. A fully developed channel velocity profile and a constant tangential velocity together with superimposed pseudo turbulent fluctuations are used as inflow conditions for the nozzle, more details about the method and its application can be taken from Klein et al. (2003a,b). The ratio of axial and tangential velocity was chosen to match the experimentally determined swirl number ($S = 0.64$). For the scalar transport equation zero flux boundary conditions are applied at the walls of the nozzle. The Reynolds number was calculated from the bulk velocity and the bluff body diameter. A co-axial air flow with a magnitude of 10% of the bulk velocity surrounds the swirler device.

The simulation as well as the experimental investigation of the scalar concentration was carried out at a Reynolds number of 5000, i.e., a bulk velocity of 2.33 m/s. In contrast, the transient velocity information has been taken from experiments running at $Re = 10{,}000$, i.e., a bulk velocity of 4.66 m/s. In order to compare this data with the DNS, the experimental data was scaled with the ratio of the corresponding Reynolds numbers. The applicability of this procedure is given, because the profiles have been found to collapse if normalized with the corresponding bulk velocity (Schneider et al., 2005) and (Freitag and Klein, 2005). The simulation run 70,000 time steps on four processors, which corresponds to 9 flow through times in terms of the bulk velocity or to 20 rotations of the coherent structure.

4. Results and discussion

In this section, the flow and the scalar field will be characterized in terms of one point statistics. The impact of the PVC on the fluid flow and mixing is then discussed by looking at spatial and temporal autocorrelations. Finally, the understanding of the complex phenomena in this configuration is enhanced by means of flow visualization techniques.

4.1. Velocity profiles

As a consequence of the relatively high swirl number, an internal recirculation zone is generated by vortex breakdown. A further consequence is the appearance of a fluid dynamic instability called precessing vortex core.

Exemplarily, Fig. 2 shows radial profiles of the mean axial velocity and the turbulent kinetic energy at different axial positions. The agreement of the simulated data with experimental data is excellent, except for a moderate under-prediction of the TKE at large radii. Also the length of the recirculation zone is well predicted as the plots of the axial velocity indicate. The high values of the turbulent kinetic energy at the axis of symmetry at $x = 1$ mm and

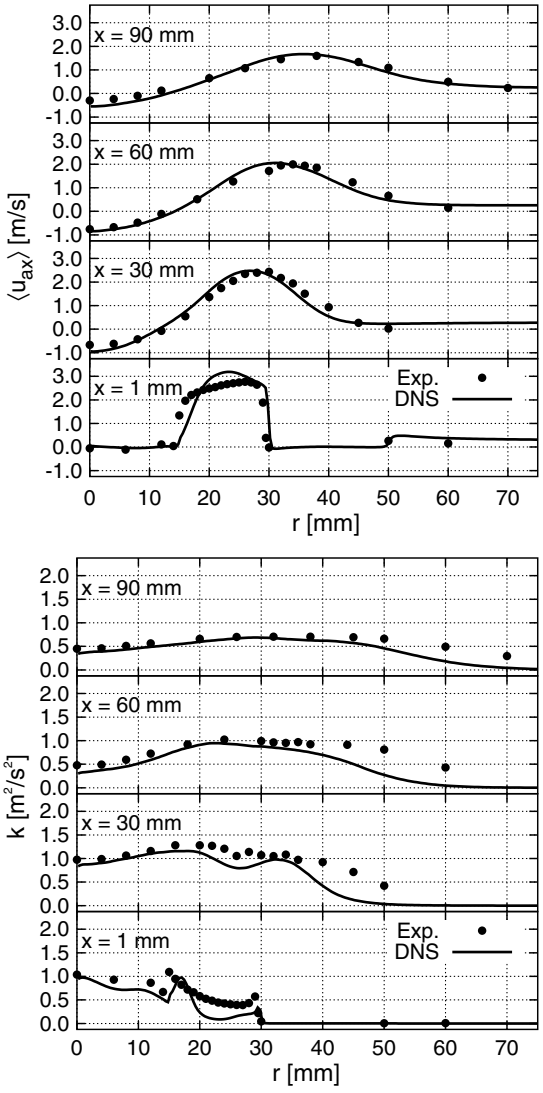

Fig. 2. Radial plots of the mean axial velocity and of the turbulent kinetic energy for selected axial positions.

$x = 30$ mm are due to the precessing motion of the coherent structure.

Other features of the flow are high shear stresses at the inner and outer edges of the annular flow issuing from the slit and a spreading of the flow pattern typical for these swirling flows. More details about the velocity field measurements and the simulation can be taken from Schneider et al. (2005) and Freitag and Klein (2005).

4.2. Scalar concentration

First and second order statistics of the scalar field have been calculated to evaluate the mixing behavior of the swirl flow. Results of the comparison between the DNS calculation and the Raman scattering can be found in Figs. 3 and 4.

The agreement of mean quantities between the calculation and the Raman measurements is very good, and also the agreement in terms of fluctuations is reasonable, considering the complexity of the flow. The underprediction of the fluctuation intensity for large radii is consistent with the underprediction of TKE, mentioned earlier. Using a Boussinesq assumption, can also explain the slightly larger spreading of the mean scalar due to a increased turbulent transport observed in the experiment.

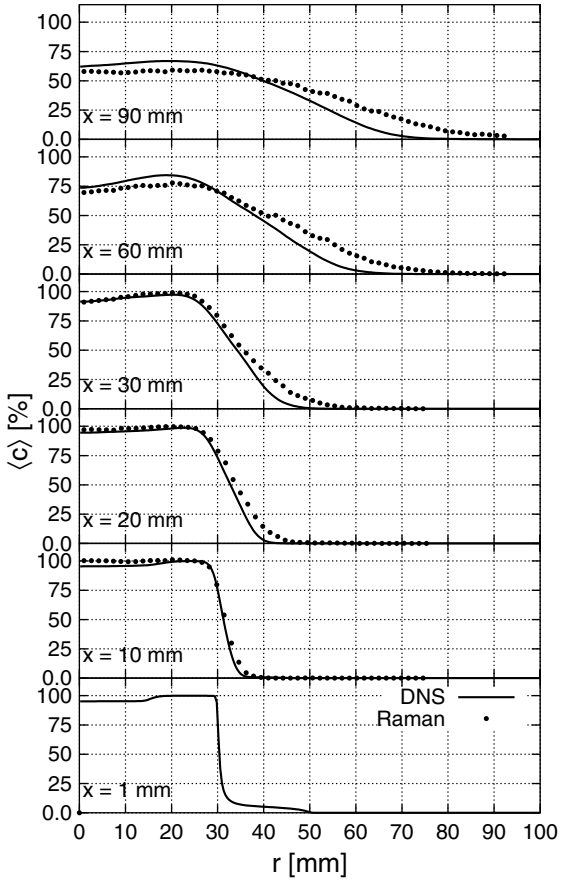

Fig. 3. Radial plots of the mean of the passive scalar for different axial positions.

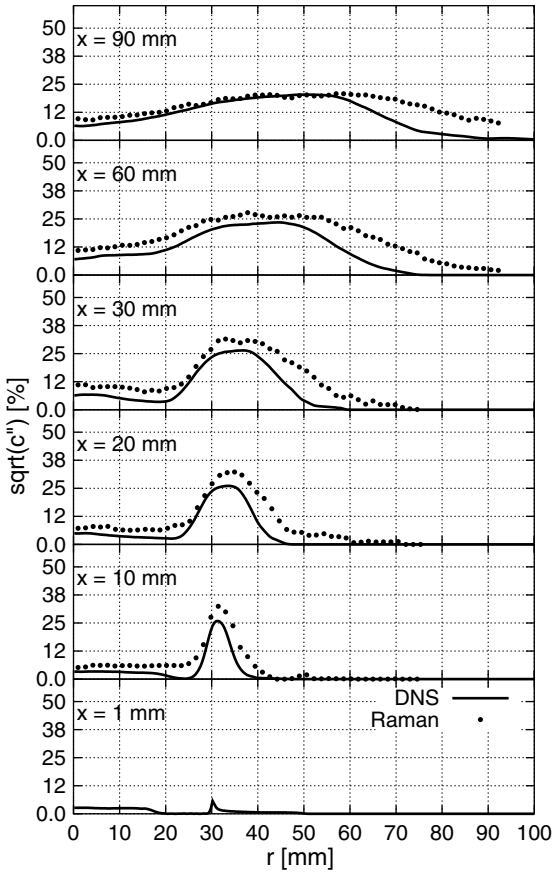

Fig. 4. Radial plots of the fluctuation of the scalar concentration for different axial positions.

4.3. Scalar transfer

Turbulent fluxes provide important information for turbulence modeling. Exemplarily Fig. 5 depicts radial plots of $\langle u'_{rad}c'\rangle$ and $\langle u'_{ax}u'_{rad}\rangle$ at different axial positions. As a general feature it can be observed that, if both are normalized, the maximum of the scalar flux is generally higher than the corresponding turbulent shear. As Chevray and Tutu (1978) found out, the bigger part of momentum and scalar transport is conducted by large scales. For small scales they concluded a better efficiency in transporting scalar than in transporting momentum. The explanation is based on the fact that the scalar is conserved, as long as molecular diffusivity is ignored. Contrarily, momentum is not conserved, because pressure forces are an additional mechanism acting on the momentum equation. Further, they assume the transport of momentum forces is achieved at the expenses of transport due to convection. Consequently, the effective mixing length for the momentum is smaller compared to the mixing length of a scalar. This yields profiles with higher magnitude for the momentum than for scalar, as can be seen in Fig. 5. This observation is consistent with the usual assumption that the turbulent Schmidt number is roughly 0.7. Lubbers et al. (2001) and Browne et al. (1984) reported similar findings for the ratio of $\langle u'_{rad}c'\rangle$ and $\langle u'_{ax}u'_{rad}\rangle$.

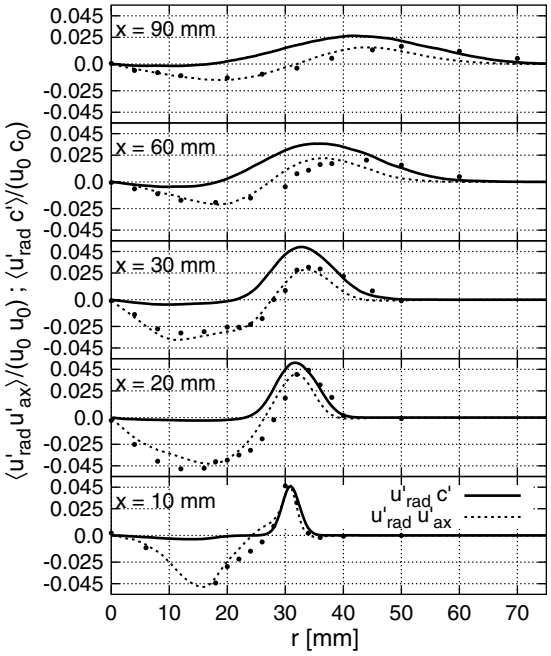

Fig. 5. Radial plots of the turbulent shear and scalar transfer for different axial positions (experimental data for the $u'_{ax}u'_{rad}$ shear correlation plotted with points).

Applying a Boussinesq assumption and using rotational symmetry, one can write

$$\langle u'_{rad}c'\rangle \sim -\frac{\partial\langle c\rangle}{\partial r} \tag{3}$$

$$\langle u'_{ax}u'_{rad}\rangle \sim -\frac{\partial\langle u_{ax}\rangle}{\partial r} - \frac{\partial\langle u_{rad}\rangle}{\partial x}. \tag{4}$$

As a general feature axial gradients of mean velocity are basically negative and considerably smaller than the radial gradients. The fact that $\langle\partial u_{ax}/\partial r\rangle$ has opposite signs in both shear layers, explains why $\langle u'_{ax}u'_{rad}\rangle$ changes sign roughly at $r = 25$ mm. Close to its maximum the turbulent shear is of a similar shape as $\langle u'_{rad}c'\rangle$ and the maxima of both correlations are located at the identical radial position. Contrarily, closer to the axis of symmetry $\langle u'_{ax}u'_{rad}\rangle$ shows a pronounced minimum, where the majority of momentum flux is drawn towards the centerline. Although one could expect the $\langle u'_{rad}c'\rangle$ distribution to exhibit a similar shape, the scalar transfer is only slightly negative. This can be explained with the almost constant mean scalar concentration, at a high level, bounding the fluctuations to a small intensity. The steep gradient of the scalar concentration at the outer nozzle edge causes the pronounced peak of the scalar flux which spreads in downstream direction.

The key property for turbulence modeling using Boussinesq's approximation is the turbulent diffusivity (3), as the constant of proportionality. Usually the turbulent diffusivity is expressed in terms of the turbulent viscosity divided by a turbulent Schmidt number. Fig. 6 shows the axial and the radial component of the turbulent diffusivity. Whereas the radial component is more or less well behaved, the axial component depicts a very strong dependence on

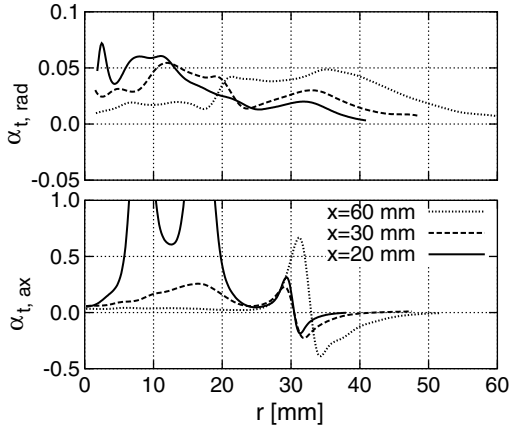

Fig. 6. Radial plots of the eddy viscosity at several axial positions.

the position in the flow. In particular the axial turbulent diffusivities are considerably larger in magnitude than the radial diffusivities due to the strong isotropy of the flow and they change sign which is an undesirable feature in the context of the Boussinesq approximation. The problematic flow regions can be identified as the outer shear layer (around $r = 30$ mm) where co-flowing air mixes with the swirl flow. Another region is located above the bluff body ($x = 20$ mm) where the PVC has been identified and where gradients of the mean scalar are very small but the turbulent fluxes are not.

4.4. Two point statistics

In addition to statistical moments two point velocity correlations with radial and axial separation have been evaluated at different positions in the flow and will be compared in this section to two point LDV measurements. The correlation functions are normalized and plotted against the separation distance normalized with the axial position as in Schneider et al. (2005) (see Fig. 7). Although both data sets still contain some statistical noise, the agreement with the experimental results, only available for the velocity correlation, is satisfactory.

By comparing the correlations at different axial positions it can be observed as a general feature that the axial length scales do not enlarge uniformly downstream, as typical in jet configurations. In that case the correlation functions would collapse, when normalized with the axial distance from the nozzle. Furthermore, the ratio of longitudinal and transverse length scale seems to be different from a ratio of 2.0 as expected for isotropic turbulence. Additional to the velocity, two point correlations of the scalar concentration have been evaluated from the DNS, see Fig. 7. They show the same features as observed for the velocity two point correlations: except for the last axial position (90 mm), the correlations are asymmetric with respect to the point of zero separation and they show strong undershoots and oscillations. The correlation for

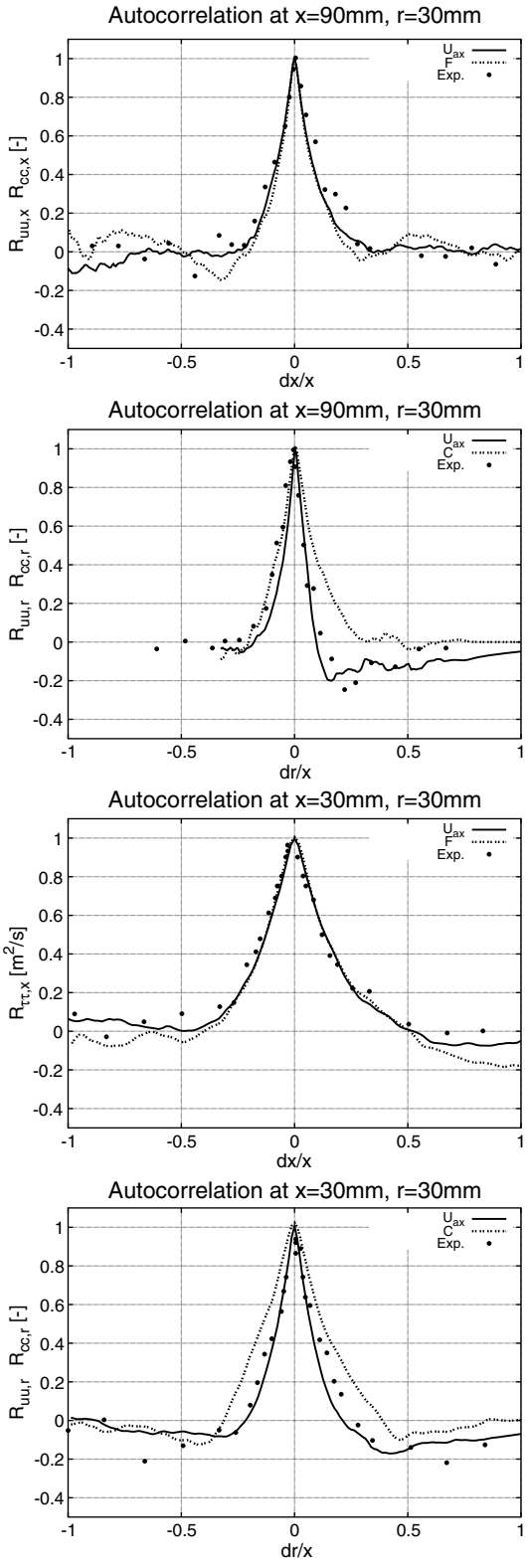

Fig. 7. Two point correlations, taken from the axial velocity and the mixture concentration, at two positions (30 mm and 90 mm downstream and 30 mm from the centerline), in comparison with experimental data.

the scalar and the velocity seems to collapse for the axial separation, but not for the radial separation, where the scalar length scale is generally bigger.

4.5. Impact of the coherent structure

As the PVC stabilizes, the precession frequency can be obtained from the temporal autocorrelation of the velocities, pressure or the transported scalar. Fig. 8 shows the spectra of the autocorrelation computed from the axial velocity at $x = 30$ mm and 20 mm away from the centerline and from the mixture concentration, at the same position. Clearly both spectra show a dominant reiterate characteristic, which arises as a peak in the computed frequency spectra at 21 Hz.

From this absolute frequency the Strouhal number $St \approx L \cdot f/U$ is calculated to compare the results with the experimental data. Taking the bluff body diameter as L and the mean bulk velocity for U we obtain a Strouhal number of $St \approx 0.27$, very close to the value of 0.25 found in the experimental investigations of Schneider et al. (2005)

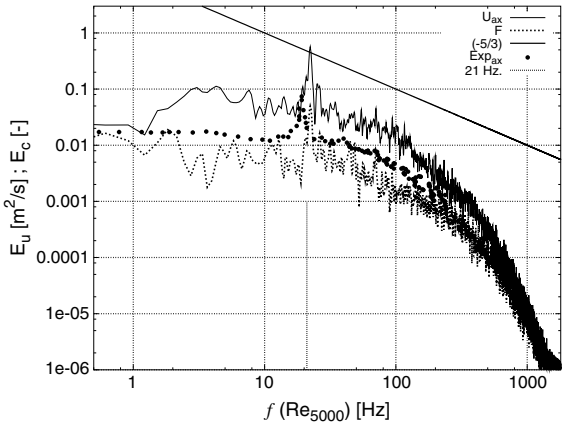

Fig. 8. Energy–density spectra of the passive scalar and of the axial velocity at a characteristic position show the frequency of the rotating structure. The experimental energy–density spectra of the axial velocity is scaled to match the Reynolds number.

Fig. 9. Plot of the pressure iso-surface to visualize the structure of the PVC (black), which wraps around the recirculating fluid (white), cutting a projection of the scalar concentration (dark grey represents high concentration).

at $Re = 10{,}000$. Due to the low repetition rate of the spontaneous Raman measurements (1 Hz), time dependent data could not be extracted. Because of the impact of the precessing vortex core, it is not surprising that the frequency can also be found in the mixture concentration. It can be observed that the PVC sucks surrounding air into the spreading cone of the flow, and thereby enhances the mixing process.

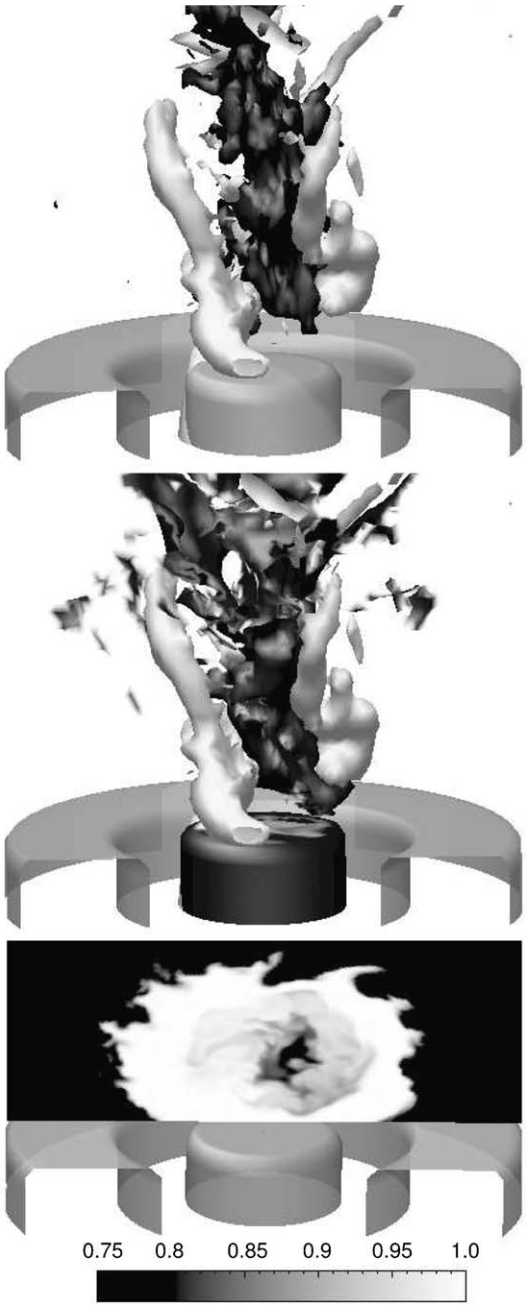

Fig. 10. 3D plots of the pressure iso-surface to visualize the structure of the PVC (white). The black iso-surface in the first plot encloses the recirculation zone and the black iso-surface in the next picture encloses a region, where the scalar concentration is less than 85%. In the third plot the scalar concentration is mapped on a plane, perpendicular to the axis of symmetry.

In Fig. 9 the coherent structure of the PVC is visualized using an iso-surface of the pressure-field ($P = P_0 - 0.25$, black shape). The recirculation zone is presented by an iso-surface of negative axial velocity (white). The scalar concentration is plotted on a plane, where dark grey represents high values and light grey low concentrations. Clearly the helical structure of the PVC can be observed. From classical vortex breakdown investigations as documented in Syred and Beer (1972) or Lucca-Negro and O'Doherty (2000) the PVC is described to encase the recirculation zone, also nicely visible in Fig. 9.

As Wegner et al. (2005) pointed out, investigating a similar type of flow, the instantaneous or phase averaged concentration of the scalar field exhibits large differences to the mean scalar concentration, especially in regions where the fluid recirculates. A similar behavior was found in the DNS results.

Fig. 10 shows instantaneous snapshots taken at the identical time and position. The upper end of the nozzle and the bluff body is included into the picture as a reference for the dimension. Also an iso-surface of the pressure-field (light grey shape), to illustrate the coherent structure of the PVC, is included in both figures.

In the upper figure the black iso-surface encloses the region of recirculating fluid, i.e., axial velocities inside the region are negative. The black iso-surface in the next figure characterizes a scalar concentration of 85%. Note that the time averaged concentration (Fig. 3) is almost 100% at the identical position. From the next snapshot, where the scalar concentration between 75% and 100% is mapped on a plane perpendicular to the axis of symmetry, it can be seen that the iso-surface of the previous figure encloses a region of concentration lower than 85% and is completely surrounded by higher scalar concentration. By comparing the position and shape of the black iso-surfaces in the upper and the middle figure, the impression is given that they almost collapse, which supports the statement that downstream the PVC draws surrounding air over a radial distance into the spreading cone of the flow and transports recirculating fluid all the way down to the bluff body, leading to considerable mixing inhomogeneities.

5. Conclusions

A DNS of a swirling recirculating flow has been performed, taking into account the transport of a passive scalar. The same configuration has been investigated experimentally at our in house facilities using LDV and Raman scattering. DNS and experiment exhibit overall a very good agreement. As a consequence of the high swirl number an internal recirculation zone is created. Furthermore, the vortex region becomes unstable forming large coherent structures precessing around the axis of symmetry. These structures lead to pronounced inhomogeneities in the instantaneous scalar field. Spatial and temporal scalar two point correlations calculated from the DNS show features similar as the velocity field. In particular coherent

structures are formed in the scalar field, precessing with the same frequency as observed in the flow field.

Using all techniques together resulted in a considerable extension of an established and well validated data base, including now detailed one point statistics, two point correlations and time series for velocity and scalar concentration under isothermal as well as under reacting conditions. Further on the database will be used to test new modeling approaches for turbulent scalar flux, as well as strategies for assessing the quality of LES as sustaining projects.

Acknowledgements

The authors gratefully acknowledge the financial support by the DFG SFB 568 (Project B1, B3 and D3) and also the DFG Project Dr374/4-1.

References

Browne, L.W.B., Antonia, R.A., Chambers, A.J., 1984. The interaction region of a turbulent plane jet. J. Fluid Mech. 149, 355–373.

Chanaud, R., 1965. Observation of oscillatory motion in certain swirling flows. J. Fluid Mech. 21, 111–127.

Chevray, R., Tutu, N.K., 1978. Intermittency and preferential transport of heat in a round jet. J. Fluid Mech. 88 (1), 133–160.

Fahler, J., Leibovich, S., 1977. Disrupted states of vortex flow and vortex breakdown. Phys. Fluids 20, 1385–1400.

Freitag, M., Klein, M., 2005. DNS of a recirculating swirling flow. Flow Turbul. Combust. 75 (1–4), 51–66.

García-Villalba, M., Fröhlich, J., 2005. On the sensitivity of a free annular swirling jet to the level of swirl and a pilot jet. In: ETMM6, 6th International Conference on Engineering Turbulence Modelling and Experiments, Sardinia.

Geyer, D., Dreizler, A., 2004. Evaluation of raman scattering experiments in hydrocarbon flames. In: Proc. Laser Applications to Chemical and Environmental Analysis.

Geyer, D., Kempf, A., Dreizler, A., Janicka, J., 2004. Scalar dissipation rates in isothermal and reactive turbulent opposed jets: Id-raman/rayleigh experiments supported by LES. Proc. Combust. Inst. 30, 681–689.

Hattori, H., Murase, Y., Nagano, Y. 2003. DNS of turbulent heat transfer in plane impigning jet. In: Hanjalic, K., Nagano, Y., Tummers, M. (Eds.), Proceedings of Turbulence, Heat and Mass Transfer 4, pp. 449–456.

Kim, J., Moin, P., 1989. Transport of passive scalars in turbulent channel flow. In: Turbululent Shear Flow, vol. VI. Springer Verlag, p. 85.

Klein, M., 2005. An attempt to assess the quality of large eddy simulations in the context of implicit filtering. Flow Turbul. Combust. 75 (1–4), 131–147.

Klein, M., Kempf, A., Sadiki, A., Janicka, J., 2004. Mixing analysis of a plane jet using direct numerical simulation. In: Euromech 10th European Turbulence Conference, July, Trondheim, Norway.

Klein, M., Sadiki, A., Janicka, J., 2003a. A digital filter based generation of inflow data for spatially developing direct numerical or large eddy simulations. J. Comp. Phys. 186, 652–665.

Klein, M., Sadiki, A., Janicka, J., 2003b. Investigation of the influence of the reynoldsnumber on a plane jet using direct numerical simulation. Int. J. Heat Fluid Flow 24/6, 785–794.

Lu, X., Sung, S.W.H., Hsieh, S., Yang, V., 2005. Large-eddy simulations of turbulent swirling flows injected into a dump chamber. J. Fluid Mech. 527, 171–195.

Lubbers, C.L., Brethouwer, G., Boersma, B.J., 2001. Simulation of the mixing of a passive scalar in a round turbulent jet. Fluid Dyn. Res. 28, 189–208.

Lucca-Negro, O., O'Doherty, T., 2000. Vortex breakdown: a review. Prog. Energy Combust. Sci. 27, 431–481.

Maanen, H.V., Nobach, H., Benedict, L., 1999. Improved estimator for the slotted autocorrelation function for randomly sampled Idv data. Meas. Sci. Tech. 10, L4–L7.

PHOENICS. Available from: <www.cham.co.uk/phoenics/d_polis/d_lecs/numerics/scheme.htm>. WWW, 2002.

Pierce, C., Moin, P., 1998. Large eddy simulation of a confined coaxial jet with swirl and heat release. AIAA 98 (2892), 1–11.

Ruith, M., Chen, P., Meiburg, E., Maxworthy, T., 2003. Three-dimensional vortex breakdown in swirling jets and wakes: direct numerical simulation. J. Fluid Mech. 486, 331–378.

Saiki, E., Biringen, S., 1996. Numerical simulation of a cylinder in uniform flow: application of a virtual boundary method. J. Comp. Phys 2 (123), 450–465.

Schneider, C., Dreizler, A., Janicka, J., 2005. Fluid dynamical analysis of atmospheric reacting and isothermal swirling flows. Flow Turbul. Combust. 74, 103–127.

Syred, N., Beer, J., 1972. The damping of precessing vortex cores by combustion in swirl generators. Acta Astronaut. 17, 783–801.

Tang, G., Yang, Z., McGuirk, J., 2002. Large eddy simulation of isothermal confined swirling flow with recirculation. Eng. Turbul. Modelling Expt. 5, 885–894.

Wegner, B., Janus, B., Sadiki, A., Dreizler, A., Janicka, J., 2005. Study of flow and mixing in a generic gt combustor using LES. In: ETMM6, 6th International Conference on Engineering Turbulence Modelling and Experiments, Sardinia.

Wegner, B., Maltsev, A., Schneider, C., Sadiki, A., Dreizler, A., Janicka, J., 2004. Assesment of unsteady rans in predicting swirl flow instability based on LES. Int. J. Heat Fluid Flow 25, 528–536.